High-Resolution NMR of an Antisense DNA·RNA Hybrid Containing Alternating Chirally Pure R_p Methylphosphonates in the DNA Backbone†

Anwer Mujeeb,‡,§ Mark A. Reynolds,||,⊥ and Thomas L. James*,‡

Departments of Pharmaceutical Chemistry and Pathology, University of California, San Francisco, California 94143-0446, and Genta, Inc., 3550 General Atomics Court, San Diego, California 92121

Received December 9, 1996⊗

ABSTRACT: A high-resolution proton NMR study has been performed on a hybrid duplex formed by a methylphosphonate (MP) oligodeoxyribonucleotide (MPO) and its target oligoribonucleotide, d($T_{MP}CC_{MP}$-$TT_{MP}AG_{MP}CT_{MP}CC_{MP}TG$)·r(CAGGAGCUAAGGA), where MP corresponds to positions of methylphosphonate linkages in the pure R_p stereoconfiguration. MP-containing analogs of DNA are reported to be effective antisense agents capable of specifically inhibiting protein synthesis with the R_p chiral MPOs exhibiting greater affinity for the target mRNA than their S_p counterparts. Nearly complete proton resonance assignments of the hybrid duplex have been made using two-dimensional nuclear Overhauser effect (2D NOE) spectra, at three different mixing times, and double quantum-filtered COSY (2QF-COSY) spectra. The 2QF-COSY cross-peak patterns which are resolved have been analyzed qualitatively to suggest sugar conformations. Distance restraints have been obtained from the 2D NOE spectra of the duplex in D_2O. These interproton distance restraints were determined using a complete relaxation matrix method to improve accuracy. Specifically, a new approach termed RANDMARDI has been utilized to calculate these distance restraints, accounting for spectral noise and errors in 2D NOE peak volume integration. The calculated interproton distances and sugar puckers have been analyzed to assess the solution conformation of the hybrid. The hybrid duplex appears to have an overall solution structure which is distinct from standard B- and A-forms, but the RNA strand exhibits features of the A-form. The absence of H1′−H2′ cross-peaks in the 2QF-COSY spectrum indicates a C3′-*endo* type of conformation for ribose sugars in the RNA strand. The deoxyriboses in the antisense DNA strand exhibit a mixed behavior with almost equal scalar coupling constant values for H1′−H2′ and H1′−H2″ and a strong H3′−H4′ 2QF-COSY peak pattern. Variations in calculated values of interproton distances and sixth-root *R* factor analysis of experimental intensities indicate that the hybrid duplex may have a DNA strand with significant conformational plasticity.

In recent years, oligodeoxyribonucleotides with modified phosphate backbones have been tested as potential antisense therapeutic agents which apparently act by inhibiting mRNA functions in living cells. These oligodeoxyribonucleotides with modified phosphate linkages can be targeted to specific sequences of mRNA to inhibit protein synthesis (Liebhaber et al., 1992; Dominski & Kole, 1993). Methylphosphonate oligodeoxyribonucleotides (MPOs)[1] are of particular interest because of their stability, enhanced resistance towards nuclease hydrolysis, and efficient permeability through mammalian cell membranes (Chem et al., 1990; Wickstorm et al., 1992; Miller, 1991; Miller et al., 1979; Agarwal & Riftina, 1979). MPO sequences complementary to initiation codons of rabbit globin mRNA have been shown to arrest translation, thus inhibiting globin synthesis (Blake et al., 1985). Antiviral activity of MPOs complementary to the acceptor splice junction in HSV-1-infected cells was indicated by reduced levels of viral DNA (Smith et al., 1986). Triple-strand-forming MPOs targeted to acetyltranferase mRNA specifically inhibit protein synthesis (Reynolds et al., 1994). Also, oligonucleotides containing MP linkages have been reported to block the induction of HIV-1 infection by targeting a U3 enhancer element in T-lymphoblastoid cell lines (Laurence et al., 1991). Methylphosphonate derivatives have also been successfully used to map the phosphate contacts which are reported to be critical for RNA recognition by HIV-1 regulatory proteins (Pritchard et al., 1994). Other DNA backbone chemical modifications have also produced antisense agents. On the basis of the biological activity demonstrated for antisense DNA agents, several have been developed to ameliorate various diseases and are currently in various stages of clinical testing.

With methyl group modification on phosphates, chiral centers are generated with either *R* or *S* chirality at the

† This work was supported by NIH Grants GM29720 and AI36636 with use of the UCSF Computer Graphics Laboratory, supported by NIH Grant RR01081, and by Genta, Inc.

* Author to whom correspondence should be addressed. Telephone: (415) 476-1569. Fax: (415) 502-4690. E-mail: james@picasso.ucsf.edu.

‡ Department of Pharmaceutical Chemistry, University of California.

§ Department of Pathology, University of California.

|| Genta, Inc.

⊥ Current address: Ribozyme Pharmaceuticals, Inc., 2950 Wilderness Place, Boulder, CO 80301.

⊗ Abstract published in *Advance ACS Abstracts,* February 15, 1997.

[1] Abbreviations: 1D, one-dimensional; 2D, two-dimensional; 2D NOE, two-dimensional nuclear Overhauser effect; 2QF-COSY, double-quantum-filtered correlation spectroscopy; EDTA, ethylenediaminetetraacetate; MP, methylphosphonate; MPO, methylphosphonate oligodeoxyribonucleotide; MP-DNA·RNA hybrid, trisdecamer hybrid duplex of DNA and RNA used in the present study with alternating R_p methylphosphonates on the DNA backbone (see Figure 1 for details); HIV-1, human immunodeficiency virus type 1; DHFR, human dihydrofolate reductase; HSV-1, herpes simplex virus type 1; rMD, restrained molecular dynamics.

S0006-2960(96)03008-5 CCC: $14.00

phosphorus. This typically results in a mixture of chemically nonequivalent oligomers. Maher and Dolnick (1988) reported that stereoselectivity of methylphosphonates plays a key role in the inhibition of human DHFR mRNA functions. The stereochemical configuration affects the stability of MP-containing DNA duplexes (Zon, 1987; Bower et al., 1987; Kibler-Herzog et al., 1991; Latha & Yathindra, 1991). Theoretical calculations have justified the differential stability (Ferguson et al., 1991; Hausheer et al., 1992). Recently, Reynolds et al. (1996) demonstrated that MPOs with R_p chiral methylphosphonate linkages bind RNA targets with higher affinity, and those with S_p linkages form weaker complexes with RNA.

Various modified oligonucleotides and their duplexes with DNA and target RNA sequences have been studied, with chemical, biochemical, and limited structural properties reported (Miller et al., 1981; LaPlanche et al., 1986; Zon, 1987; Agarwal et al., 1989; Uhlmann & Peyman, 1990; González et al., 1994, 1995). There has, however, been no structure established so far for any methylphosphonated DNA·RNA hybrid duplex.

Indeed, very little is known about antisense oligonucleotide structure in general. There is, for example, an X-ray structure of a DNA octamer containing a single 3′-methylene phosphonate (diastereomeric mixture) (Heinemann et al., 1991). Several years ago, we performed NMR studies on a DNA octamer containing a single phosphorothioate in which some structural effects of the different chiralities could be inferred (LaPlanche et al., 1986). More recently, we obtained the solution structures of two hybrid DNA·RNA duplexes, differing only in the chirality of the single phosphorothioate in the DNA strand (González et al., 1994, 1995). An NMR structural study of a self-complementary DNA with a single phosphorodithioate found that the modification induces significant distortion (Cho et al., 1993). More interesting from the perspective of development of antisense oligonucleotides perhaps would be studies in which several backbone phosphodiesters were modified. Quite recently, a self-complementary DNA dodecamer sequence with either all phosphorodithioates or all phosphorothioates (as a diastereomeric mixture) was studied using NMR (Jaroszewski et al., 1996). Evidence of hairpin formation and reduced base pair lifetimes was found.

In the present paper, we have carried out a high-resolution proton NMR study of d($T_{MP}CC_{MP}TT_{MP}AG_{MP}CT_{MP}CC_{MP}$-TG)·r(CAGGAGCUAAGGA), a 13-base pair hybrid duplex of methylphosphonated DNA and RNA (MP-DNA·RNA). Alternate phosphodiesters (marked with a subscript MP) on the DNA strand were modified to methylphosphonodiesters in the chirally pure R_p configuration. The R_p chiral analogues were chosen, as their complexes are reported to be more stable than those with the S_p configuration (Reynolds et al., 1996; Bower et al., 1987). An alternating arrangement of chirally pure MP and phosphodiester linkages on the antisense DNA strand hybridizes better to RNA than racemic mixtures (Reynolds et al., 1996). Nearly all proton resonance assignments on the MP-DNA·RNA hybrid could be made via 2D NOE and 2QF-COSY spectra. Structural characterization followed from interproton distances determined via complete relaxation matrix analysis of 2D NOE spectra and from sugar puckers evaluated via analysis of cross-peak patterns in 2QF-COSY spectra.

MATERIALS AND METHODS

Sample Preparation. The chemical synthesis of methylphosphonate DNA composed of alternating chirally pure MP and phosphodiester linkages has recently been described (Reynolds et al., 1996). Strands of chirally pure R_p methylphosphonate DNA and RNA were mixed in a 1:1 stoichiometry, and the formation of hybrid duplex was monitored using UV spectrophotometry. The hybrid duplex was buffered in 10 mM phosphate buffer at pH 6.9, 20 mM sodium chloride, and 0.25 mM EDTA. The solution was heated at 85 °C for 3 min and slowly cooled to room temperature. An equal quantity of additional buffer was added during cooling of the sample. The final duplex concentration was about 1.5 mM.

NMR Experiments. All NMR spectra were acquired at 500 MHz using a General Electric GN-500 NMR spectrometer. NMR data processing was performed on Sun workstations using UCSF NMR software: STRIKER and SPARKY 3.0. All 2D NMR experiments were performed at 30 °C, except 2D NOE experiments in 90% H_2O/10% D_2O which were run at 10 °C. Pure absorption phase 2D NOE spectra in D_2O were acquired in hypercomplex mode (States et al., 1982) with a spectral width of 5000 Hz in both dimensions. There were 2K points in the ω_2 dimension and 512 points in the ω_1 dimension. In each experiment, 16 scans were collected per t_1 value, and a repetition time of 10 s was used between acquisitions to minimize saturation. The data were processed with a Gaussian window function and zero-filled to achieve a final size of 2K × 2K. Three 2D NOE data sets were collected, each with a mixing time of 50, 150, or 350 ms.

For resonance assignments of imino and amino exchangeable protons, 2D NOE experiments in 90% H_2O/10% D_2O were carried out using 11ECHO (Sklenar & Bax, 1987) and NODE-1 (Liu et al., 1993) pulse sequences. A mixing time of 150 ms was used with a spectral width of 10 000 Hz. The probe temperature for these experiments was 10 °C.

Pure absorption-doubled quantum-filtered COSY (2QF-COSY) spectra were acquired using TPPI phase cycling (Marion & Wüthrich, 1983). There were 2048 and 800 data points in the ω_2 and ω_1 dimensions, respectively. The spectral width was 5000 Hz in both dimensions, the number of scans 32, and the repetition delay 3 s. A 30°-shifted sine bell window function was applied during processing of 2QF-COSY data.

Spin−lattice relaxation times (T_1) for protons in the MP-DNA·RNA hybrid were measured via the inversion−recovery method utilizing a 180° composite pulse (Freeman et al., 1980). A total of 25 spectra were acquired using variable delays. In each experiment, 64 scans were collected with a repetition delay time of 30 s. Spin−spin relaxation times (T_2) were estimated by the spin-echo method (Hahn, 1950) using the same acquisition parameters as for T_1 experiments.

Measurement of 2D NOE Cross-Peak Intensities and Generation of Distance Restraints. Integration of 2D NOE peak volumes was performed using SPARKY 3.0 software. SPARKY allows quantitation of peak volumes for overlapping peaks by line-fitting methods (González et al., 1995). Cross-peaks on both sides of the diagonal were integrated, and an average value of the two intensities was utilized for subsequent interproton distance calculations.

There are several methods of analyzing 2D NOE spectra to obtain interproton distances. We have found that use of a complete relaxation matrix approach allows determination of distance restraint bounds with good accuracy (Borgias & James, 1988, 1990; Thomas et al., 1991; Liu et al., 1995). The program MARDIGRAS employs this approach in an iterative fashion using the geometry of a starting structure to account for 2D NOE intensities that are not available from experimental data. It has been demonstrated several times that the program manifests very little dependence on the starting structure (Borgias & James, 1990; Schmitz et al., 1990; Weisz et al., 1992; Mujeeb et al., 1992) while yielding reliable distances. In the present case, three initial models were used as starting structures for each mixing time data set in MARDIGRAS calculations.

Starting Model Structures. A set of starting model structures was generated for MARDIGRAS. Three models were generated: standard A-form, standard B-form, and a third structure with the DNA strand in the B conformation and the RNA strand in the A conformation. This heteronomous model structure of the MP-DNA·RNA hybrid necessitated DNA strand sugars in the O4′-*endo* conformation with pseudorotation angles (*P*) around 96°. Sugar conformations on the RNA strand were modeled as C3′-*endo* with pseudorotation angles around 28°. The molecular modeling software package SYBYL (from Tripos, St. Louis) and the program DNAminiCarlo (Ulyanov et al., 1993) were used to generate these structures. Methylphosphonates on the DNA strand backbone were modeled in the R_p configuration using the following values of dihedral angles involving the methyl carbon atom: C3′−O3′−P−C_{MP} as 120° and C_{MP}−P−O5′−C5′ as 50°. Model structures were energy-minimized with AMBER 4.0 (Pearlman et al., 1991). A 1000-step energy minimization using a combination of steepest descent and conjugate gradient methods was performed in each case. Backbone charges on phosphates were reduced to −0.2 to implicitly account for counterion condensation (Mujeeb et al., 1993). The partial atomic charges and force field parameters for methylphosphonates were as reported by Ferguson and Kollman (1991). A distance-dependent dielectric constant was used to mimic bulk solvent effects. These calculations were performed on a cluster of Hewlett-Packard (HP-735) computers.

MARDIGRAS Calculations. A single correlation time, assuming isotropic motion, was used for tumbling of the whole molecule. Calculations were performed with 2, 3, and 4 ns, encompassing the experimentally estimated range of correlation time (*vide infra*). A three-state jump model was used for the methyl proton's internal motions (Liu et al., 1992). Distance bounds derived from multiple MARDIGRAS runs using data from the three mixing times, the three starting models, and the three correlation times were utilized to obtain refined structures via preliminary rMD calculations. These refined structures were recycled as starting structures for additional MARDIGRAS calculations to yield more accurate distances; while the calculated distances are not greatly affected by starting structure, accuracy is improved with better starting structures.

All intensities were used for calculation of the normalization factor used in MARDIGRAS. This normalization factor is used during MARDIGRAS calculations to scale the experimental to the theoretical intensities. The RANDMARDI algorithm (*vide infra*) was applied during MARDIGRAS calculations to account for spectral noise and peak integration errors (Liu et al., 1995).

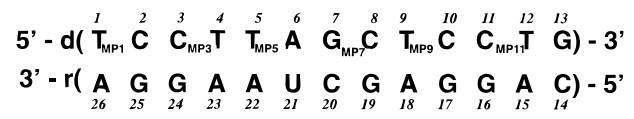

FIGURE 1: Numbering of nucleotides in the MP-DNA·RNA hybrid. Methylphosphonate groups have been assigned the same number as their 5′-neighboring nucleotide.

Quantitation of interproton distances from NOE cross-peak intensities can be compromised by decreased signal to noise and by integration errors (Liu et al., 1995). Distance errors resulting in noise and integration errors are exacerbated for 2D NOE intensities measured at longer mixing times, when "spin diffusion" is significant; calculated distances are typically underestimated (Liu et al., 1995). While a complete relaxation matrix approach largely removes spin diffusion errors (Borgias & James, 1990), more accurate upper and lower bounds for interproton distances result if one takes the intensity errors into account in MARDIGRAS calculations. A new approach to this, termed RANDMARDI (random error MARDIGRAS), was recently developed (Liu et al., 1995) and has been applied in the present study. Random noise and integration errors, estimated realistically but conservatively by the user, are introduced into the intensity data set, and the modified intensities are used by MARDIGRAS to calculate distances and bounds. MARDIGRAS calculations with *N* randomly modified sets of intensities, especially when used with experimental 2D NOE data from three mixing times and with three different estimates of the correlation time, yield a large number of distance values from which upper and lower bounds can be determined. This procedure was successfully applied to a DNA−psoralen complex and produced accurate distance bounds corroborated by resulting values for 20 fixed and known distances (Liu et al., 1995).

R Factor Calculations. The complete relaxation matrix program CORMA can be used to compare experimental 2D NOE cross-peak intensities with values calculated for any structure. To monitor the fit of experimental and calculated intensities, a residual index analogous to a crystallographic *R* factor could be used. But this *R* factor is dominated by cross-peaks corresponding to very short distances. A more sensitive monitor of fitting all NOE cross-peaks is the sixth-root residual index, R^x factor, which is based on the sixth-root dependence of 2D NOE intensities on distances (Thomas et al., 1991). R^x factors were calculated for the three 2D NOE data sets obtained at different mixing times using the three model structures of the MP-DNA·RNA hybrid described above. R^x factor values for each individual residue were analyzed to evaluate the fit of each model structure to the experimental data. R^x factors were also determined from redacted lists of cross-peaks involving solely intraresidue or interresidue interactions. These were anticipated to aid us in assessing the conformational preferences of individual nucleotides.

RESULTS AND DISCUSSION

Proton Resonance Assignments. The nucleotides in the MP-DNA·RNA hybrid are numbered as shown in Figure 1. Chirally pure methylphosphonate moieties in the R_p configuration were given the same number as their 5′-neighboring

Table 1: Chemical Shifts (Parts per Million) of Different Protons in the MP-DNA·RNA Hybrid at 30 °C[a]

residue	NH[b]	H6/H8/MP	H5/Me/H2	H1′	H2′	H2″	H3′	H4′	H5′/5″
MP-DNA strand									
T1	13.63	7.65	1.84	6.19	2.49	2.64	5.10	4.25	3.82
MP1		1.76							
C2		7.74	5.93	6.14	2.40	2.70	4.72	4.40	−
C3		7.57	5.54	6.03	2.16	2.72	4.76	4.35	−
MP3		1.78							
T4	14.04	7.34	1.55	6.16	2.38	2.63	5.12	4.41	4.23/4.19
T5	13.14	7.56	1.67	6.15	2.56	2.68	5.27	4.37	4.20
MP5		1.84							
A6		7.89	7.90	6.07	2.40	2.47	4.66	4.22	−
G7	13.09	7.77		6.20	2.21	2.65	5.19	4.25	−
MP7		1.79							
C8		7.48	5.39	6.09	2.27	2.58	5.09	4.35	4.19/4.15
T9	12.65	7.30	1.52	6.07	2.21	2.65	4.82	4.44	4.33
MP9		1.75							
C10		7.50	5.59	5.92	2.54	2.67	5.20	4.46	4.21
C11		7.09	5.08	5.77	2.21	2.60	4.41	4.33	
MP11		1.79							
T12	13.94	7.61	1.46	6.21	2.53	2.58	5.17	4.37	4.16
G13	13.19	7.49		5.96	2.28	2.63	4.60	4.34	−
RNA strand									
C14		7.96	5.48	5.37	4.51		4.28	3.99	3.90
A15		8.19	7.32	6.00	4.83		4.51	4.21	3.99/3.89
G16	12.29	7.24		5.58	4.61		4.41	4.14	4.08
G17	12.60	7.19		5.70	4.55		4.49	4.32	4.08
A18		7.73	7.66	5.54	4.76		4.62	4.40	4.13/4.09
G19	12.27	7.23		5.51	4.49		4.42	4.38	4.07
C20		7.63	5.16	5.44	4.59		4.44	4.93	4.08
U21	13.46	7.96	5.87	5.49	4.65		4.61	4.41	4.12
A22		8.13	6.45	5.85	4.73		4.53	4.44	4.21
A23		7.91	6.79	5.83	4.68		4.57	4.47	4.16
G24	12.71	7.16		5.51	4.48		4.42	4.38	4.07
G25	12.61	7.48		6.15	4.49		4.40	4.34	4.20
A26		7.90	8.10	6.06	4.15		4.08	4.32	4.30

[a] Blank spaces denote the fact that assignments are not applicable and dash marks an unassigned resonance. [b] Chemical Shifts at 15 °C.

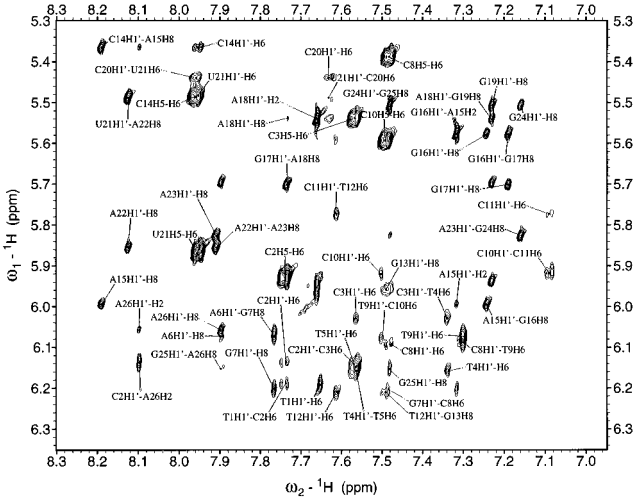

FIGURE 2: Aromatic−H1′ cross-peak region of the 2D NOE spectrum (350 ms mixing time) of the MP-DNA·RNA hybrid in D_2O at 30 °C.

nucleotide. Sequential resonance assignments of nonexchangeable protons on the MP-DNA·RNA hybrid duplex were made in 2D NOE spectra at 50, 150, and 350 ms mixing times following standard sequential resonance assignment strategies. Chemical shifts of proton resonances are listed in Table 1.

As an example, resonance assignments in the aromatic−H1′ region of a 2D NOE spectrum are shown in Figure 2. The anchor point for the sequential walk in the DNA strand was the identification of methyl groups on thymines at positions 1, 4, 5, 9, and 12 (Figure 1). Strong intranucleotide cross-peaks were observed between thymine methyl protons and TH6 protons. Except residue T1, each of the methyl resonances exhibited a sequential internucleotide cross-peak to the H6 proton of the 5′-neighboring base. For residues T4, T9, and T12, additional strong 2D NOE peaks were observed between methyl groups of these thymines and H5 protons of their 5′-adjacent cytosines: C3, C8, and C10, respectively. It should be noted that sequential H5−methyl distances are shorter (∼3.3 Å) for A-type conformations. Assignments were then followed for cross-peaks between H6 and H5 protons of neighboring cytosines. Positions of H5−H6 cross-peaks in cytosines and methyl−H6 cross-peaks in thymines were confirmed in 2QF-COSY spectra. The H5−H6 cross-peak of residue U21 was distinguished on the basis of a sequential base−H1′ walk. Once T-methyl protons and base H6 and H5 protons were identified, the sequential walk was sought in the base−H1′ region. Assignments of T-CH_3 protons were then followed in the H_2O 2D NOE spectrum, where these protons exhibited intraresidue cross-peaks to N3H imino protons on thymines. This is an intranucleotide covalent interproton distance of ∼4.9 Å. Weak cross-peaks in water 2D NOE spectra were also observed between methyl protons on thymines and the cross-strand 5′-neighbor's imino protons. Exchangeable imino and amino protons were assigned in the water 2D NOE spectrum (Rajagopal et al., 1988; Zhou et al., 1988). A sequential network of cross-peaks could be successfully traced for exchangeable imino protons starting at residue T1. The imino proton on each thymine manifested a strong cross-peak to the H2 proton of the base-paired adenine. These imino−adenine H2 proton cross-peaks helped in unambigu-

ous assignment of individual AH2 proton resonances, previously identified as such by their long T_1 relaxation times and cross-strand NOEs to H1′ protons.

Assignments of deoxyribose spin systems in the DNA strand were accomplished by combined use of 2QF-COSY and 2D NOE spectra. Despite substantial overlap in the H1′−H2′/H2″ region, all spin systems were identified and assigned. In RNA duplexes, A-type helices are expected which have ribose sugars in the C3′-*endo* conformation. In the C3′-*endo* conformation, the H1′−H2′ scalar coupling is less than 2−3 Hz. Due to such a small coupling, H1′−H2′ cross-peaks are not observed in 2QF-COSY spectra of duplex RNA. The lack of cross-peaks between H1′ and H2′ protons poses a major obstacle in assigning RNA sugar resonances. With the MP-DNA·RNA hybrid, only one H1′−H2′ 2QF-COSY cross-peak was observed on the RNA strand, that for the 3′-end terminal residue A26. This readily indicates that, as typically observed in RNA duplexes, a C3′-*endo* conformation is manifested by riboses in the RNA strand. Residue A26, being the 3′-terminal residue on the RNA strand, might be experiencing enhanced conformational flexibility with a finite population of C2′-*endo* ribose, thus enabling observation of the H1′−H2′ cross-peak in 2QF-COSY spectra. Such behavior of 3′-terminal residues is common in RNA duplexes as well as in RNA strands of hybrids (Varani & Tinoco, 1991; González et al., 1994). Identification of the A26 residue's H1′ and H2′ proton chemical shifts in this manner constituted a reliable way of starting sequential assignments in the RNA strand. 2D NOE data were used to assign RNA base and sugar protons. Strong intranucleotide NOE's were seen between H1′ and H2′ protons at short (50 ms) mixing times. This NOE corresponds to an A-type conformation, where the H1′−H2′ distance is around 2.6−3.0 Å. Strong sequential H8/H6−H2′ NOEs were observed in the RNA strand. In an A-type conformation, these strong NOEs correspond to a short distance of ∼2.0 Å. Conversely, intranucleotide H2′−H6/H8 NOEs were weaker, as expected for the A-form. NOE cross-peaks were also found between H5 protons on pyrimidine residues and their 5′-neighbor's H2′ and H3′ protons. In addition, H3′ protons on ribonucleotides also displayed sequential cross-peaks to the H6/H8 base protons.

Adenine H2 proton resonances were first identified by their relatively long T_1 relaxation times (Mujeeb et al., 1992; González et al., 1994) in inversion recovery experiments. Using 2D NOE spectra acquired with the hybrid in H_2O, H2 proton resonances were assigned to particular adenines on the basis of strong thymine imino−adenine H2 NOEs. Sequential 2D NOEs from H2 protons were then followed in the base−H1′ region, where each of these protons exhibited sequential connectivities to the H1′ proton of the 3′-neighbor and also, in some cases, cross-strand NOEs to the nucleotide base-paired on the 5′-side. For example, cross-peaks were seen between A6H1′ and A22H2 and between A15H2 and G16H1′ protons. Such cross-peaks would certainly be expected for an A-form helix. In the DNA strand, there are sporadic suggestions of an A-form helix, e.g., the presence of an A6H3′−G7H8 NOE.

NOEs involving the methylphosphonates were also evident in our 2D NOE spectra. These methyl groups exhibited cross-peaks with sugar protons in neighboring residues. Figure 3 exemplifies MP−H3′ cross-peaks in a 2D NOE spectrum. A representation of possible interactions of R_p methylphosphonate protons with other protons which can give rise to NOEs is given in Figure 4. These contacts were indeed found in 2D NOE spectra of the MP-DNA·RNA hybrid. Cross-peaks with medium to weak intensity were seen between the methylphosphonate and the H3′ and H4′ protons of 5′-neighboring residues. For example, we observed weak 2D NOE cross-peaks between the T1H3′ proton and MP at position 1. Other such cross-peaks observed were T4H3′−MP4, T5H3′−MP5, G7H3′−MP7, C10H3′−MP9, and T12H3′−MP11. In model structures of the hybrid, these distances for the R_p configuration of methylphosphonate range from 4.0 to 5.2 Å. In contrast, for the S_p configuration, one would expect a strong NOE between the H3′ proton and the methylphosphonate CH_3 group as this distance is around 2.8 Å. The weak to medium cross-peak intensities confirm the R_p configuration. In some cases, the methyl group on MPs also exhibited cross-peaks to the H3′ proton of the 3′-neighbor; for example, MP7 showed a weak cross-peak to C8H3′ in the 350 ms spectrum. In a heavily overlapped region, methylphosphonates also showed cross-peaks to H5′/H5″ protons of the 3′-residue. These distances in model structures range from 2.99 to 3.75 Å, depending on the modeled conformation.

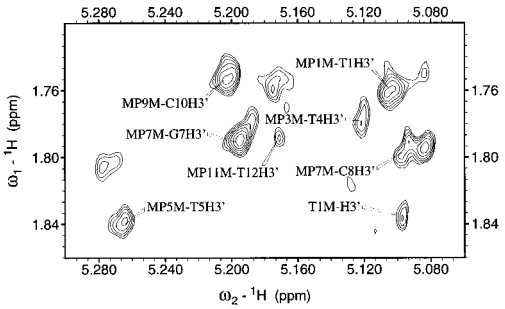

FIGURE 3: H3′−methylphosphonate NOEs in the 2D NOE spectrum (350 ms mixing time) of the MP-DNA·RNA hybrid in D_2O at 30 °C.

Relaxation Time Measurements and Estimation of Correlation Time. The measurements of spin−lattice relaxation times (T_1) and spin−spin relaxation times (T_2) were made by 1D NMR methods. These measurements mainly helped in identifying adenine H2 protons and H1′ protons on the RNA strand and with an estimation of the overall correlation time of the MP-DNA·RNA hybrid. T_1 relaxation times measured for base and H1′ protons are listed in Table 2. Adenine H2 protons have T_1 values longer than others in nucleic acids due to the limited proton density around them (Mujeeb et al., 1992; González et al., 1994). Longer T_1 values for H1′ protons on RNA, especially relative to DNA, have also been reported earlier and are attributed to the lack of H2″ protons in ribose sugars relative to deoxyriboses in the DNA strand. This is in accord with earlier reports of T_1 values of such protons in DNA·RNA hybrids (Wang et al., 1992; González, 1994). A single correlation time can be estimated from measured T_1 and T_2 values (Suzuki et al., 1986). An average value for the correlation time of the MP-DNA·RNA hybrid was 2.5 ± 1.0 ns according to this method. In subsequent MARDIGRAS calculations, assuming isotropic motion, correlation times of 2.0, 3.0, and 4.0 ns were used.

Analysis of 2QF-COSY Data. Heavy signal overlap in the deoxyribose H1′−H2′/H2″ region of the 2QF-COSY spectrum precluded quantitative estimation of coupling constants using our conventional methods (Weisz et al., 1993; Mujeeb et al., 1992; Schmitz et al., 1990). However, a qualitative

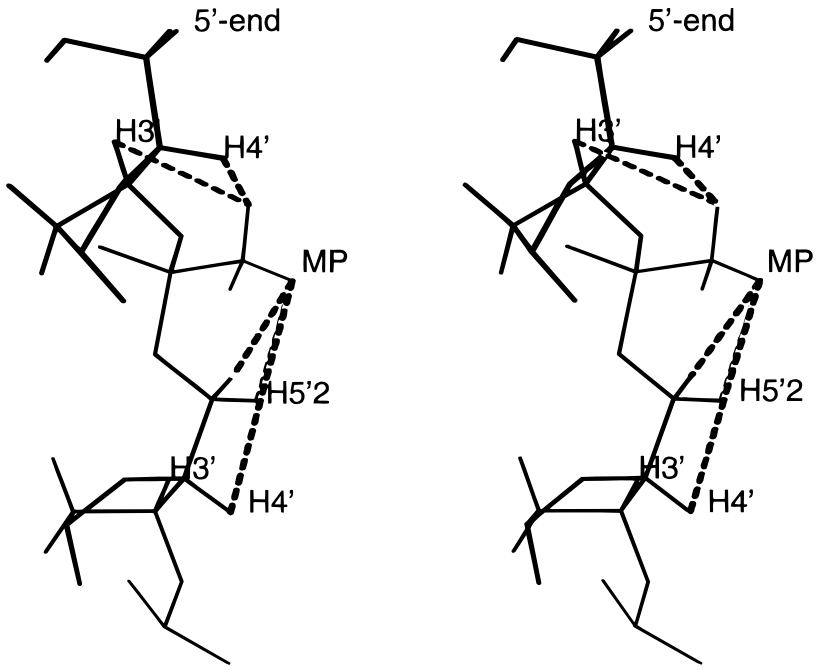

FIGURE 4: Stereoview of the backbone of an energy-minimized conformation of a dinucleotide unit in B-form containing a methylphosphonate in the R_p configuration. Interproton distances (<5 Å) involving the methyl group of MP are drawn as broken lines.

Table 2: Spin−Lattice Relaxation Times (T_1) of Protons on the MP-DNA·RNA Hybrid at 30 °C

proton(s)	T_1 (s)	proton(s)	T_1 (s)
T1 and C2H1′	1.8	C14H6	4.3
T1H6	2.9	A15H1′	4.7
C3H1′	2.2	A15H8 and H2	3.6
C3 and T5H6	1.8	G16 and G17H1′	4.7
T4 and T5H1′	1.8	G16 and G17H8	4.3
A6H1′	2.5	A18H2 and H1′	4.6
A6H8	3.3	A18H8	3.6
A6H2	3.6	G19H8 and H1′	4.3
G7H1′	1.8	C20H1′	5.4
G7H8	2.2	U21H6 and H1′	4.3
C8H1′	2.8	A22H1′	5.4
C8H6	3.6	A22H8 and H2	5.0
C8H5	3.3	A23H2 and H1′	5.1
T9H1′	2.5	A23H8	4.0
T9H6	2.2	G24H1′	4.3
C10H1′	2.1	G25H8 and H1′	4.3
C11H6 and H1′	2.2	A26H1′	4.7
T12H6 and H1′	1.8	A26H8	3.3
G13H1′	2.9	A26H2	4.3

analysis of peak patterns is in order. As mentioned above, riboses in the RNA strand showed 2QF-COSY patterns typical of a C3′-*endo* (N domain) sugar conformation. The absence of H1′−H2′ COSY peaks due to smaller coupling is a hallmark of N conformations. For deoxyriboses, we have observed strong H3′−H4′ couplings along with an almost similar peak pattern for H1′−H2′ and H1′−H2″ cross-peaks. The H1′−H2″ 2QF-COSY cross-peaks have fine structure with only four components, unlike a predominantly S domain pucker which exhibits a 16-peak pattern (Mujeeb et al., 1992; Schmitz et al., 1990). This is indicative of similar coupling constants for H1′−H2′ and H1′−H2″ couplings in deoxyriboses. COSY cross-peaks were also observed for H2″−H3′. Such peak patterns were also reported by González et al. (1994) for another DNA·RNA hybrid. Although some of these cross-peak patterns can be explained by a rigid O4′-*endo* (E-type) conformation (Salazar et al., 1993b), a consideration of all cross-peaks for a particular deoxyribose in the hybrid could be explained better by a dynamic model of deoxyribose repuckering (González et al., 1995), in which sugars were found to repucker rapidly between N and S conformations. Peak overlap prevents a rigorous analysis in the present case, but a similar situation cannot be ruled out and would be consistent with other analysis (*vide infra*).

Analysis of NOE Distance Restraints Extracted by MARDIGRAS Analysis. Interproton distances are sensitive to three-dimensional molecular structure. As the energetically feasible structural variations for right-handed oligonucleotide duplexes is not too great, many of the distances between pairs of protons may differ only slightly for different possible conformations. Consequently, to distinguish between the different potential structural forms, we find it necessary to determine from 2D NOE experiments as many interproton distances as possible with the greatest accuracy possible. To achieve this, we have used the complete relaxation matrix approach in the MARDIGRAS algorithm (Borgias & James, 1988, 1990). This method takes into account indirect magnetization transfer effects (spin diffusion) and yields accurate interproton distances from measured 2D NOE intensities. However, interproton distance calculations are further complicated by the fact that the measured intensities of 2D NOE peaks have errors from integration as well as spectral noise. This influences weak NOE intensities more, as they are more strongly affected by spectral noise and are difficult to integrate accurately, being particularly sensitive to the choice of the base plane. As these weak NOE cross-peaks correspond to longer interproton distances, they are quite important to structure determination. In the present case, such distances involve the MP methyl group, as weak cross-peaks were observed between methyl protons and neighboring H3′ and H4′ sugar protons (*vide supra*). To accommodate the effects of spectral noise and integration errors during interproton distance calculations, we adopted a new approach termed RANDMARDI (Liu et al., 1995). This approach has been shown to yield accurate upper and lower bounds for the distances, in particular from weak

Table 3: Statistical Overview of Conformations Preferred by Residues in the MP-DNA·RNA Hybrid Based on Sixth-Root *R* Factors (R^x) in CORMA Calculations[a]

	MP-DNA strand								RNA strand							
	50 ms		150 ms		350 ms				50 ms		150 ms		350 ms			
residue	inter	intra	inter	intra	inter	intra	overall	residue	inter	intra	inter	intra	inter	intra	overall
T1	B/H	B/H	B	B	B/H	B/H	B/H	A26	H	A/H	H	H	A/H	S	A/H
C2	H	S	B	H	B	B/H	B/H	G25	A	A/H	A/H	H	B	H	A/H
C3	S	S	B	S	A/H	A/H	B/H	G24	B	H	H	A/H	S	H	A/H
T4	S	S	S	S	S	A/H	A/B/H	A23	B	S	S	S	A/H	B	A/B/H
T5	A	B	B	B	B	B/H	B	A22	A/H	S	H	S	A/H	B	A
A6	S	S	S	S	S	S	A/B/H	U21	B	S	A	A/B	A/H	A/H	A
G7	A	B/H	A	A/H	S	A	A/B	C20	A/H	A/H	A/H	S	A/H	B/H	A/H
C8	A	B/H	A	B	A	S	A/B	G19	H	B	A/H	S	A/H	B	A/H
T9	H	B/H	S	B/H	A/B	S	B/H	A18	H	H	A	A/H	H	A/H	A/H
C10	B	S	H	B/H	A	B/H	B/H	G17	H	A	A	A	A/H	A/H	A/H
C11	A/B	S	S	A	A	A	A/B	G16	S	H	A	A	A	B	A
T12	A	H	H	B	A	B/H	A/B/H	A15	H	A	B	A/H	B	S	A/H
G13	A	S	B	B/H	S	S	A/B/H	C14	B/H	B/H	S	S	A	A	A/B/H

[a] A, B, and H represent the model structure for which the per residue R^x factor is lowest; S is where R^x factor value is comparable for all three (A, B, and H) model structures.

intensities, by taking into account the above-mentioned effects.

We obtained distance restraints independently from three 2D NOE data sets acquired at 50, 150, and 350 ms mixing times. Three starting structures and three correlation time values of 2, 3, and 4 ns were used for each intensity data set during RANDMARDI calculations. Each RANDMARDI calculation was comprised of 30 MARDIGRAS runs with randomization of experimental intensities (Liu et al., 1995). Each of the 27 calculations provided upper and lower bounds for distances. The final distances and their bounds were obtained by averaging the results of all 27 individual calculations. A total of 360 distance restraints (each with a lower and upper bound) consisting of 232 intranucleotide, 126 internucleotide, and 2 interstrand restraints were obtained. There were 12 restraints involving methylphosphonates. Due to the lack of H2″ protons, the number of restraints for the RNA strand was relatively less than that for the DNA strand.

Analysis of Sixth-Root R Factors. Sixth-root *R* factor calculations were carried out for all three mixing time data sets against the three model structures of the MP-DNA·RNA hybrid. For each individual residue, experimental intensities were categorized as intraresidue or interresidue, and R^x values corresponding to these categories were compared for the three model structures using intensities for each of the three mixing times individually. In each case, the best fit is indicated by the lowest R^x value among the three model structures. More precisely, a comparatively low R^x value indicates that the 2D NOE intensities are more in accord with the corresponding model conformation. We performed such an analysis of preferred conformation for each individual residue; results are presented in Table 3. On the whole, the MP-DNA strand residues prefer either the B- or H-form. Some residues on the DNA strand show comparable values of R^x factor for all three conformations (indicated by S in Table 3). Possibly, these residues are capable of attaining more than one conformation equally well, a suggestion of flexibility in the DNA strand. In the RNA strand, mostly A-form is preferred. It should be noted that, in the H-model structure, the RNA strand was designed in pure A-form; thus, an overall fit to H-form in the RNA strand indirectly refers to an A-type conformation. It is evident via per residue R^x analysis that the MP-DNA strand displays more conformational heterogeneity than the RNA strand, which seems to mostly stay in an A-type conformation.

Structural Implications of Measured Interproton Distances. There is very little published information about the structure of any antisense oligonucleotides bound to their target RNA. By analogy with the enhanced stability of RNA homoduplexes compared to DNA homoduplexes, antisense oligonucleotides with modified backbones that permit the RNA strand to retain its A-type helicity would be predicted to have enhanced binding affinity. It has been found that MPOs with R_p linkages bind more strongly than those with S_p linkages (or racemic mixtures) (Reynolds et al., 1996). Computer modeling suggests that the S_p chiral methyl groups can point into the major groove and consequently may affect the structure. In this context, it may be worth noting that our initial studies on a hybrid duplex containing an antisense MPO with the sequence reported here entailed a racemic mixture. All two-dimensional NMR spectra for that racemic duplex, obtained under a variety of conditions, exhibited broad signals due to chemical shift heterogeneity (K. Weisz, unpublished data). In other words, resonances from protons distant from the methyl group were broadened, due to superimposition of spectra from each of the individual duplexes comprising the racemic mixture; the slightly different chemical shifts leading to the observed broadening apparently arise from slight structural differences among those chiral cousins.

We have analyzed the interproton distances to assess the structural character of the R_p chiral MP-DNA·RNA hybrid. Some structurally significant experimental distances were compared to corresponding values in the three models. The experimental distances, as well as those from models A, B, and H, are listed in Table 4. Sequential H2′−H1′ NOE contacts can only be observed in the A-form, and they have been observed in the RNA strand. In A-form, this distance is about 4.0 Å. Calculated values for H2′−H1′ distances in the RNA strand are similar to the value expected for an ideal A-form. As discussed above, the A-type conformation of the RNA strand in MP-DNA·RNA is also supported by the presence of sequential and interstrand adenine H2−H1′ contacts and by 2QF-COSY results.

Intrasugar distance values measured for the DNA strand can elucidate conformational preferences for the deoxyri-

Table 4: Average Experimental Interproton Distances (Angstroms) Calculated via MARDIGRAS[a]

distance	average value in DNA strand (SD)[b]	average value in RNA strand (SD)	ideal value in A-form	ideal value in B-form	ideal value in H-form
H2′−H1′$_{interresidue}$	−	3.67 (0.48)	4.00	−	4.00
H1′−H4′$_{intraresidue}$	3.25 (0.30)	3.60 (0.55)	3.60	3.60	2.80
H2′−H6/H8$_{interresidue}$	2.96 (0.55)	2.70 (0.48)	2.40	3.60	2.40
H2′−H6/H8$_{intraresidue}$	2.80 (0.49)	2.93 (1.37)	3.60	2.10	2.70
H2"−H6/H8$_{interresidue}$	3.20 (0.62)	−	3.60	2.10	2.70
H2"−H6/H8$_{intraresidue}$	3.06 (0.59)	−	4.40	3.60	4.10
H3′−H6/H8$_{interresidue}$	3.80 (0.42)	2.80 (0.31)	3.30	4.80	4.40
H3′−H6/H8$_{intraresidue}$	3.73 (0.75)	2.99 (0.28)	3.00	4.30	4.30

[a] For comparison, ideal values of corresponding distances in three model structures are listed. [b] Standard deviation in interproton distance values.

boses. Although the H1′−H4′ distance is about the same (∼3.6 Å) for pure C2′-*endo* (S domain) and C3′-*endo* (N domain) sugar conformations, lower values (∼2.4 Å) would be expected for E-type ($P \sim 90°$) conformations. Experimental values corresponding to H1′−H4′ distances in deoxyriboses generally tend to be slightly shorter than in riboses, but they are not nearly short enough to correspond to an E-type conformation (Table 4). In principle, H2″−H4′ distances of deoxyriboses could discriminate between different conformations, as values for S-, N-, and E-type conformers are ∼3.8, ∼2.4, and ∼2.9 Å, respectively. Unfortunately, peak overlap permitted only three H2″−H4′ distances to be measured, those in residues T9, C10, and T12. These varied from 3.0 to 3.7 Å. These values clearly do not correspond to deoxyribose conformations characteristic of A-DNA but are most suggestive of values anticipated for B-DNA.

Intra- and interresidue distances involving H2′ and H6/H8 base protons exhibit substantial variation among the three model conformations. The experimental interresidue H2′−H6/H8 distances of the DNA strand listed in Table 4 largely adopt an intermediate value between those of A and B conformations. In the RNA strand, these distances stay close to the A-type value in general, with a few residues closer to the ideal B conformation value. The intraresidue H2′−H6/H8 distances display mixed behavior but are mostly clustered around the H-type value of 2.7 Å. Additional information about the DNA strand conformation can be obtained from sequential H2″−H6/H8 distances. For the MP-DNA·RNA hybrid, these distances either agree with H-form or tend toward the A-form value. Conversely, intraresidue H2″−H6/H8 distances seem to be closer to a value corresponding to a B-type conformation. Such dichotomous behavior of the deoxyribose interproton distances suggests that there are varying levels of conformational averaging in different nucleotides of the DNA strand.

Internucleotide H3′−H6/H8 contacts in the DNA strand exhibit larger variations and are shorter than in standard B-form, but the corresponding distances in the RNA strand are much shorter than those typical of A-form. Similar behavior of H3′−H6/H8 distances was observed in other DNA·RNA hybrids (González et al., 1994). Distances between H3′ and base protons reflect sugar pucker parameters as well as glycosidic bond rotation angles (González et al., 1994; Ulyanov et al., 1994; Wijmenga et al., 1993) and require careful interpretation. The short H3′−H6/H8 distances for the RNA strand are consistent with all other data indicating that strand is A-like. For the DNA strand, the situation is somewhat unclear, as distances are certainly shorter than those of B-form. On the basis of only these observations, an E-type sugar conformation (Salazar et al., 1993) cannot be ruled out; however, there is also the possibility of rapid exchange of deoxyriboses between N and S conformers. In an earlier study of a DNA·RNA hybrid in this laboratory, similar distances were measured for DNA strand deoxyriboses, again consistent with an E conformation (González et al., 1994, 1995). However, coupling constants were definitely not consistent with an E conformer, but could only be explained when a rapid exchange between N and S sugar domains was taken into account. A bimodal conformational envelope with variations both in populations as well as sequence-dependent details of the nucleotide conformations would also explain the fairly large variation in distances (3.5−4.3 Å) measured for the DNA strand in the MP-DNA·RNA hybrid.

CONCLUSIONS

We have performed 2D NMR experiments on a tris-decamer DNA·RNA hybrid, d($T_{MP}CC_{MP}TT_{MP}AG_{MP}CT_{MP}CC_{MP}TG$)·r(CAGGAGCUAAGGA), with alternating R_p methylphosphonates on the DNA strand. Assignments of proton resonances were made for all except a few H5′/5″ protons. All six methylphosphonates were assigned and displayed NOEs expected for the R_p configuration. Cross-peak intensities from 2D NOE spectra were analyzed to yield interproton distances using a new improved algorithm to account for noise and integration errors in the iterative relaxation matrix method MARDIGRAS. This method yielded about 360 experimental distance restraints, i.e., 7−24 restraints per residue, including interresidue and interstrand restraints. The calculated distances were compared to interproton distances in three different models of the hybrid to assess overall structural characteristics. The RNA strand manifested interproton distances typical of A-type structure; the general lack of 2QF-COSY cross-peaks for riboses is also consistent with A-type structure. However, interproton distances and 2QF-COSY cross-peak patterns indicate that the DNA strand nucleotides are in neither the standard A- nor B-type conformation. The available data, limited by spectral peak overlap, are consistent with the deoxyribose sugars either being in an E-type ($P \sim 90°$) conformation or experiencing rapid conformational jumps between N- and S-type conformations. It is noteworthy, however, that previous work with a DNA·RNA hybrid exhibiting better spectral dispersion found that all the data could be accounted for only by invoking conformational flexibility in the DNA strand (González et al., 1994, 1995). A sixth-root-based residual factor analysis of experimental 2D NOE intensities was successfully used to generate an overview of the conformational preferences of individual residues.

ACKNOWLEDGMENT

The authors acknowledge Dr. Klaus Weisz for initial work on the project and Dr. Nikolai Ulyanov for generating the hybrid model structure and many helpful discussions. We also acknowledge use of the Computer Graphics Laboratory at the University of California, San Francisco.

REFERENCES

Agarwal, K. L., & Riftina, F. (1979) *Nucleic Acids Res. 6*, 3009−3024.

Agarwal, S., Goodchild, J., Civeira, M., Sarin, P. S., & Zamecnik, P. C. (1989) *Nucleosides Nucleotides 8*, 819−823.

Blake, K. R., Murakami, A., Spitz, S. A., Glave, S. A., Reddy, M. P., Ts'o, P. O. P., & Miller, P. S. (1985) *Biochemistry 24*, 6139−6145.

Borgias, B. A., & James, T. L. (1988) *J. Magn. Reson. 79*, 493−512.

Borgias, B. A., & James, T. L. (1990) *J. Magn. Reson. 87*, 475−487.

Bower, M., Summers, M. F., Powell, C., Shinozuka, K., Regan, J. B., Zon, G., & Wilson, W. D. (1987) *Nucleic Acids Res. 12*, 4915−4931.

Chem, T. L., Miller, P. S., Ts'o, P. O. P., & Colvin, O. M. (1990) *Drug Metab. Dispos. 18*, 815−818.

Cho, Y., Zhu, F. C., Luxon, B. A., & Gorenstein, D. G. (1993) *J. Biomol. Struct. Dyn. 11*, 685−702.

Chou, S. H., Flynn, P., & Reid, B. (1989) *Biochemistry 28*, 2435−2443.

Diminski, Z., & Kole, R. (1993) *Proc. Natl. Acad. Sci. U.S.A. 90*, 8673−8677.

Ferguson, D. M., & Kollman, P. A. (1991) *Antisense Res. Dev. 1*, 243−254.

Freeman, R., Kempsell, S. P., & Levitt, M. H. (1980) *J. Magn. Reson. 38*, 453−479.

Giles, R. V., & Tidd, D. M. (1992) *Nucleic Acids Res. 20*, 763−770.

González, C., Stec, W., Kobylanska, A., Hogrefe, R. I., Reynolds, M. A., & James, T. L. (1994) *Biochemistry 33*, 11062−11072.

González, C., Stec, W., Reynolds, M. A., & James, T. L. (1995) *Biochemistry 34*, 4969−4982.

Hahn, E. L. (1950) *Phys. Rev. 80*, 580−594.

Hausheer, F. H., Rao, B. G., Saxe, J. D., & Singh, U. C. (1992) *J. Am. Chem. Soc. 114*, 3201−3206.

Heinemann, U., Rudolph, L.-N., Alings, C., Morr, M., Heikens, W., Frank, R., & Blocker, H. (1991) *Nucleic Acids Res. 19*, 427−433.

Jaroszewski, J. W., Clausen, V., Cohen, J. S., & Dahl, O. (1996) *Nucleic Acids Res. 24*, 829−834.

Kibler-Herzog, L., Zon, G., Uznanski, B., Whittier, G., & Wilson, W. D. (1991) *Nucleic Acids Res. 19*, 2979−2986.

LaPlanche, L. A., James, T. L., Powell, C., Wilson, W. D., Uznanski, B., Stec, W. J., Summers, M. F., & Zon, G. (1986) *Nucleic Acids Res. 14*, 9081−9093.

Laurence, J., Sikder, S. K., Kulkosky, J., Miller, P., & Ts'o, P. O. P. (1991) *J. Virol. 65*, 213−219.

Liebhaber, S. A., Russell, J. E., Cash, F. E., & Eshleman, S. S. (1992) in *Gene Regulation: Biology of Antisense RNA and DNA* (Erickson, R. P., & Izant, J. G., Eds.) pp 163−175, Raven Press, New York.

Liu, H., Thomas, P. D., & James, T. L. (1992) *J. Magn. Reson. 98*, 163−175.

Liu, H., Weisz, K., & James, T. L. (1993) *J. Magn. Reson. A 105*, 184−192.

Liu, H., Spielmann, H. P., Ulyanov, N. B., Wemmer, D. E., & James, T. L. (1995) *J. Biomol. NMR 6*, 390−402.

Maher, L. J., & Dolnick, B. J. (1988) *Nucleic Acids Res. 16*, 3341−3358.

Marion, D., & Wüthrich, K. (1983) *Biochem. Biophys. Res. Commun. 113*, 967−974.

Miller, P. S. (1991) *Bio/Technology 9*, 358−362.

Miller, P. S., Yano, J., Yano, E., Carroll, C., Jayaraman, K., & Ts'o, P. O. (1979) *Biochemistry 18*, 5134−5143.

Miller, P. S., McParland, K. B., Jayaraman, K., & Ts'o, P. O. (1981) *Biochemistry 20*, 1874−1880.

Miller, P. S., Agris, C. H., Aurelian, L., Blake, K. R., Murakami, A., Reddy, M. P., Spitz, S. A., & Ts'o, P. O. P. (1985) *Biochimie 67*, 769−776.

Mujeeb, A., Kerwin, S. M., Egan, W., Kenyon, G. L., & James, T. L. (1992) *Biochemistry 31*, 9325−9338.

Mujeeb, A., Kerwin, S. M., Kenyon, G. L., & James, T. L. (1993) *Biochemistry 32*, 13419−13431.

Murakami, A., Blake, K. R., & Miller, P. S. (1985) *Biochemistry 24*, 4041−4046.

Pearlman, D. A., Case, D. A., Caldwell, J. C., Seibel, G. L., Singh, U. C., Weiner, P., & Kollman, P. A. (1991) AMBER 4.0, University of California, San Francisco.

Pritchard, C. E., Grasby, J. A., Hamy, F., & Zacharek, A. M. (1994) *Proc. Natl. Acad. Sci. U.S.A. 22*, 2592−2600.

Rajagopal, P., Gilbert, D. E., van der Marel, G. A., van Boom, J. H., & Feigon, J. (1988) *J. Magn. Reson. 78*, 526−537.

Reynolds, M. A., Arnold, L. J., Almazan, M. T., Beck, T. A., Hogrefe, R. I., Metzler, M. D., Stoughton, S. R., Tseng, B. Y., Trapane, T. L., Ts'o, P. O. P., & Woolf, T. M. (1994) *Proc. Natl. Acad. Sci. U.S.A. 91*, 12433−12437.

Reynolds, M. A., Hogrefe, R. I., Jaeger, J. A., Schwartz, D. A., Riley, T. A., Marvin, W. B., Daily, W. J., Vaghefi, M. M., Beck, T. A., Knowles, S. K., Klem, R. E., & Arnold, L. J., Jr. (1996) *Nucleic Acids Res.* (in press).

Salazar, M., Champoux, J. J., & Reid, B. R. (1993a) *Biochemistry 32*, 739−744.

Salazar, M., Fedoroff, O. Y., Miller, J. M., Ribeiro, N. S., & Reid, B. R. (1993b) *Biochemistry 32*, 4207−4213.

Schmitz, U., Zon, G., & James, T. L. (1990) *Biochemistry 29*, 2357−2368.

Sklenar, V., & Bax, A. (1987) *J. Magn. Reson. 74*, 469−479.

Smith, C. C., Aurelian, L., Reddy, M. P., Miller, P. S., & Ts'o, P. O. P. (1986) *Proc. Natl. Acad. Sci. U.S.A. 83*, 2787−2791.

States, D. J., Haberkorn, R. A., & Ruben, D. J. (1982) *J. Magn. Reson. 48*, 286−292.

Suzuki, E., Pattabiraman, N., Zon, G., & James, T. L. (1986) *Biochemistry 25*, 6854−6865.

Swarnalatha, Y., & Yathindra, N. (1993) *J. Biomol. Struct. Dyn. 10*, 1023−1045.

Thomas, P. D., Basus, V. J., & James, T. L. (1991) *Proc. Natl. Acad. Sci. U.S.A. 88*, 1237−1241.

Uhlmann, E., & Peyman, A. (1990) *Chem. Rev. 90*, 543−584.

Ulyanov, N. B., Schmitz, U., & James, T. L. (1993) *J. Biomol. NMR 2*, 547−568.

Ulyanov, N. B., Schmitz, U., Kumar, A., & James, T. L. (1995) *Biophys. J. 68*, 13−24.

Varani, G., & Tinoco, I. (1991) *Rev. Biophys. 24*, 479−532.

Wang, A. C., Kim, S. G., Flynn, P., Chou, S. H., Orban, J., & Reid, B. (1992) *Biochemistry 31*, 3940−3946.

Weisz, K., Shafer, R. H., Egan, W., & James, T. L. (1992) *Biochemistry 31*, 7477−7487.

Wickstrom, E., Bacon, T. A., & Wickstrom, E. L. (1992) *Cancer Res. 22*, 6741−6745.

Wijmenga, S. S., Mooren, M. M. W., & Hilbers, C. W. (1993) in *NMR in Macromolecules* (Roberts, G. C. K., Ed.) pp 217−288, IRL Press, Oxford.

Zhou, N., Manogaran, S., Zon, G., & James, T. L. (1988) *Biochemistry 27*, 6013−6020.

Zon, G. (1987) *J. Protein Chem. 6*, 131−145.

BI963008N